

Structural Design Analysis Torque Links of Nose Landing Gear on Light Aircraft

Arif Krisbudiman ^{a,*}, Khairu Rezqi ^a, Rismu Landung Gumilang ^a, Mohamad Dahsyat ^b, Harris Zenal ^a
Andi Muhdiar Kadir ^a, Edy Yulianto ^c

^a Research Center for Structural Strength Technology, National Research and Innovation Agency, Raya PUSPIPTEK, Science and Technology Area B.J. Habibie, Serpong, Building 220, Setu, South Tangerang 15314, Indonesia

^b Research Center for Process and Manufacturing Industry Technology, National Research and Innovation Agency, Raya PUSPIPTEK Science and Technology Area B.J. Habibie, Serpong, Technology Building 2, Setu, South Tangerang 15314, Indonesia

^c Indonesian Nuclear Technology Polytechnic, Babarsari, Ngentak, Caturtunggal, Depok District, Sleman Regency, Special Region of Yogyakarta 55281, Indonesia

Corresponding author: *arif027@brin.go.id

Abstract—Torque links are components of Nose Landing Gear on the designed lightweight aircraft, that connect between the inner and outer cylinders of an oleo-pneumatic shock strut. They prevent torsion or twisting between those components and vibrations at retractable nose landing gear, the safety of these components is very important, especially when landing aircraft. This paper studies the stress and deformation contours of the torque link design with variations of hole geometry to get the optimal design, with the lightest possible weight but still reliable and safe. The upper torque link is modeled as a simply supported beam with a moment on one end derived from impact force when landing. Maximum bending stresses occur in areas near holes and the connection part of the torque link. This analysis with a tetra mesh by changing the hole position and geometry. The final torque link design results in a weight reduction of up to 23.75% with a maximum stress is 157.4 MPa and displacement is 0.0166 mm. Torque link design optimization results are then modally analyzed, and four natural frequencies and the mode shape are done. The natural frequency of vibration of different mode shapes obtained ranges from 4.2259 kHz to 6.1319 kHz, and this is still below the limit of 0.1 kHz (around 6,000 rpm engine). Finally, the optimal design torque links were obtained, safe from static and dynamic loads with a Factor of Safety 1.78 (>1.5) according to the FAR-23 standard.

Keywords— Design optimization; modal analysis; nose landing gear; structural analysis; torque links.

Manuscript received 24 Jul. 2023; revised 20 Dec. 2023; accepted 13 Jan. 2024. Date of publication 30 Apr. 2024.
IJASEIT is licensed under a Creative Commons Attribution-Share Alike 4.0 International License.



I. INTRODUCTION

The aircraft landing gear is an assembly that supports the aircraft on the ground, enabling it to safely take off, land, and taxi [1]. Torque links are one of the major components of landing gear, which take more impact loading during landing [2]. The landing gear system is one of the most important systems in an aircraft [3]. The torque links performed by the analysis are nose landing gear on PUNA aircraft. PUNA is a Medium Altitude Long Endurance (MALE) Unmanned Aerial Vehicle (UAV) designed by Agency for Technology Assessment and Application. Nose retractable landing gear on PUNA aircraft is to take the wheels of the aircraft both on landing and when turning left and right.

Nose retractable landing gear on PUNA aircraft can be seen in Figure 1, complete with its components. The nose wheel can be pulled into the body of the aircraft with a retractable system while it is flying and can be pushed out when the aircraft is about to land. Its movement is carried out by linear actuators very carefully so as not to damage other components of the aircraft. Integration of several subsystems into an existing structural assembly can lead to significant mass and volume reduction, which subsequently improves measures such as range, speed, and fuel efficiency of air transportation vehicles [4], [5]. All analysis of landing gear mechanisms on PUNA aircraft is very important including torque links.

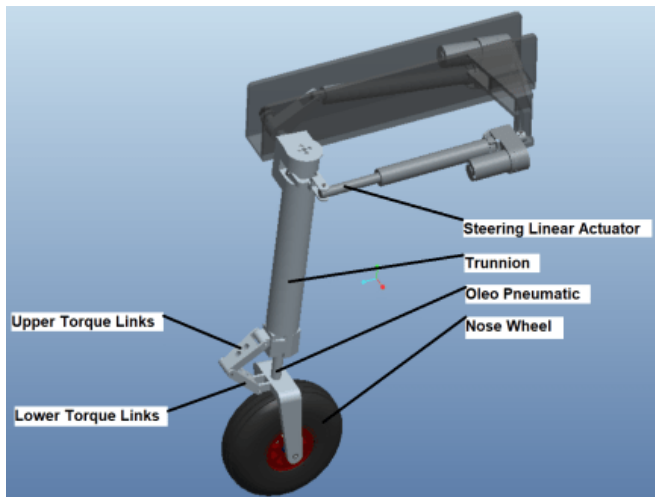


Fig. 1 Retractable nose landing gear

The geometry is altered keeping in mind the objective of reducing weight and maximum stress. In the landing gear assembly of an aircraft, the torque links connect the two telescoping cylinders and prevent the relative rotation of the piston to maintain the wheel alignment during taxiing on the ground [6]. It tries to obtain a general trend in the variation of stresses and keep the volume at a minimum value. The mechanical model of the NLG system is mainly composed of force elements such as air spring force, oil damping force, structural limiting force, tire force, and torsional damping force [7]. A modal analysis is also performed on the optimized models. Landing gears are subject to large sources of vibration during take-off and landing. Phanikrishna, Bernad, and Mark [2] did a study on the onset of shimmy oscillation of an aircraft landing gear to find the regions of stable torsional and shimmy oscillations. Identifying the natural frequencies and mode shapes of torsion links is essential to avoid resonance. The available literature on the study of torsion links is very little in number. In the work done by FatmaKocer, topology optimization of torsion links is done to reduce overall weight [3]. The initial model has two holes as shown in Figure 2. This study will help engineers reduce the weight of components by removing material from the main component. The study by Arravind, Saravanan, and Rijuwan uses carbon fiber in composite materials to design, optimize, and analyze composite torsion links [8]. In this study, structural analysis of torque links of nose landing gear on light aircraft based on static and dynamic loads was carried out both theoretically and through the Finite Element Method to obtain an optimal design.

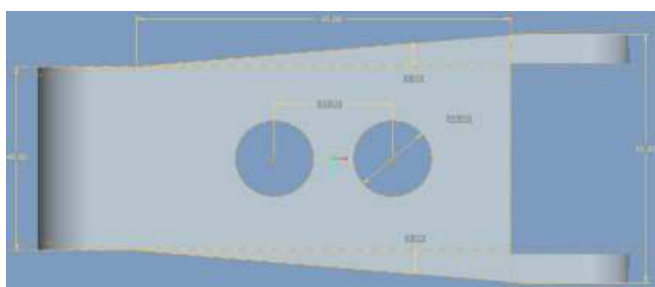


Fig. 2 Initial model of torque link

Torque Links analysis is conducted by looking at Von Mises Stress and Displacement that occurs due to static loads and dynamic loads while operating. Static loads on torque links can be calculated from the weight of the aircraft. Dynamic loads can be calculated from the energy absorbed by the oleo-strut shock absorber when the plane lands. The line of work of static load and dynamic load is right on the oleo-pneumatic axis line of the nose landing gear in the downward direction. These static loads (F_{static}) and dynamic loads ($F_{dynamic}$) can be described as static moment (M_{static}) and dynamic moment ($M_{dynamic}$) at torque links (Figure 3) [9]. Torque Links structural analysis is performed to determine the maximum stress that occurs due to static and dynamic loads. And can be a reference in the iteration of shape modification if necessary to get optimal design. In design verification and product development, prototype modeling plays a unique role in improving product quality, shortening time to market, and in turn increasing profitability [10]. The hinge clearance and rotation axis deviation of aircraft landing-gear retraction mechanism are unavoidable due to factors, such as manufacture, assembly, wear, and wing deformation [11].

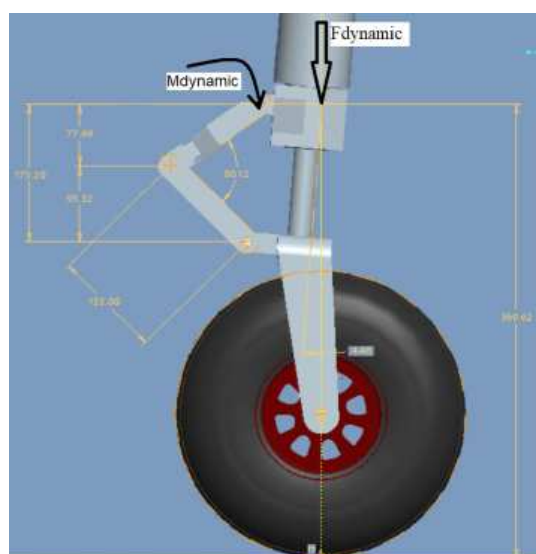
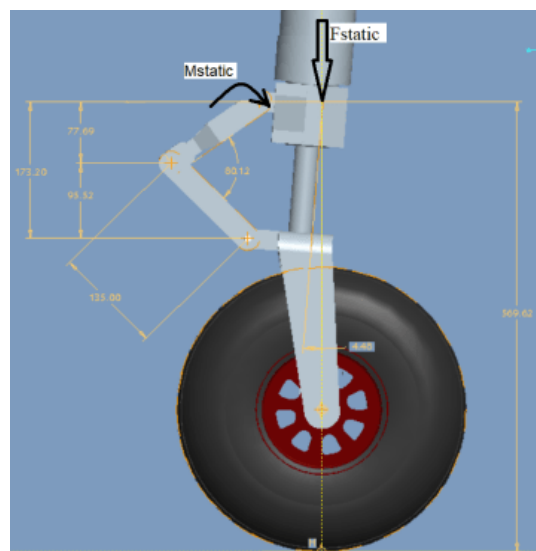


Fig. 3 Initial model of torque link

II. MATERIALS AND METHOD

The nose landing gear is an aircraft component that protects the structure from the impact loads that occur during landing. The impact load will be dampened by the shock absorbers before then being transmitted to the nose landing gear structure. The occurrence of resonant bifurcations can induce tire-ground vibrations in torsional and lateral directions, which can greatly degrade the performance and safety and possibly destroy the airstrip [12]. The conventional type of landing gear system for UAVs consisting of a linear spring and damping system has some limitations. Significant stiffness in the landing gear system can improve the steering stability; however, the transmission force becomes significant, thus increasing the acceleration response of the UAV body. This side effect can cause damage to the landing gear structure and UAV components. Conversely, a low-stiffness landing gear system can reduce the force transmission and acceleration of the UAV. However, the UAV static deflection becomes large, and the steering stability reduces. Practically, the landing gear's static displacement is limited by the landing gear's space and dimensions [13], [14]. Torque links are one of the main components of the nose landing gear which receives the impact load, so a structural strength analysis of torque links is needed to get the optimal design.

Nose landing gear uses shock absorbers to absorb kinetic energy when the aircraft lands or touchdowns at a certain speed. The touchdown kinetic energy is very important because it can affect the structural strength of the landing gear. Using a representative high-fidelity Multi-Body Dynamic model and numerical solution scheme in the time domain, 3D shimmies maps and 2D stability boundaries are obtained and employed to understand the nonlinear phenomena of interest, contributing to more realistic performance estimation of nose landing gears in early design stages [4]. For landing gear design, it is assumed that all the energy at touchdown is absorbed by the shock absorber and the tires are as follows. Different joint clearances have different effects on shimmy: the joint clearance between the NLG and fuselage has little influence on shimmy; the larger axial clearance of upper and lower torque link joint will cause the shimmy of the NLG, but the radial clearance has no effect on shimmy; while the joint clearance between turning sleeve and upper torque link, lower torque link and piston only work in the axial and radial coupling [15]. Shock absorber configuration using oil and gas, from that configuration, makes static deflection large and reduces steering stability (see equation 1):

$$\text{Based equation} = W_L N_g (h_t S_t + h_s S_s) \quad (1)$$

$$S_s = \left[\left(\frac{v_z^2}{2gN_g} \right) - h_t S_t \right] / h_s \quad (2)$$

Then, a stroke of the shock absorber with a safety margin in feet (S_s_design) can be determined by (see equation 3):

$$S_s_design = S_s + 1/12 \quad (3)$$

Static force in Newton (F_{static}) can be determined with the maximum static load at the nose landing gear being 15% of the Maximum Take-Off Weight (MTOW):

$$\begin{aligned} P_m &= 15\%W_L \\ F_{static} &= P_m g \end{aligned} \quad (4)$$

Assumed that by definition: $WL = n_s P_m$. Dynamic force in Newton ($F_{dynamic}$) can be determined as follows (see equation 5):

$$F_{dynamic} = [n_s P_m N_g (h_t S_t + h_s S_s_design)] g \quad (5)$$

Torque Links analysis is done by creating solid 3D images, and then calculating static loads and dynamic loads that work on torque links. Based on solid 3D images, existing load, and boundary conditions, stress analysis is done by previously meshing first. Stress analysis shows which areas experience the greatest and what is the maximum deformation on the design of torque links. Then iterations of modification of the shape or thickness of torque links, so that the maximum stress that occurs is still below the material yield strength and deformation, with a safety factor above 1.5 [16], [17]. The process flow steps can be seen in Figure 4.

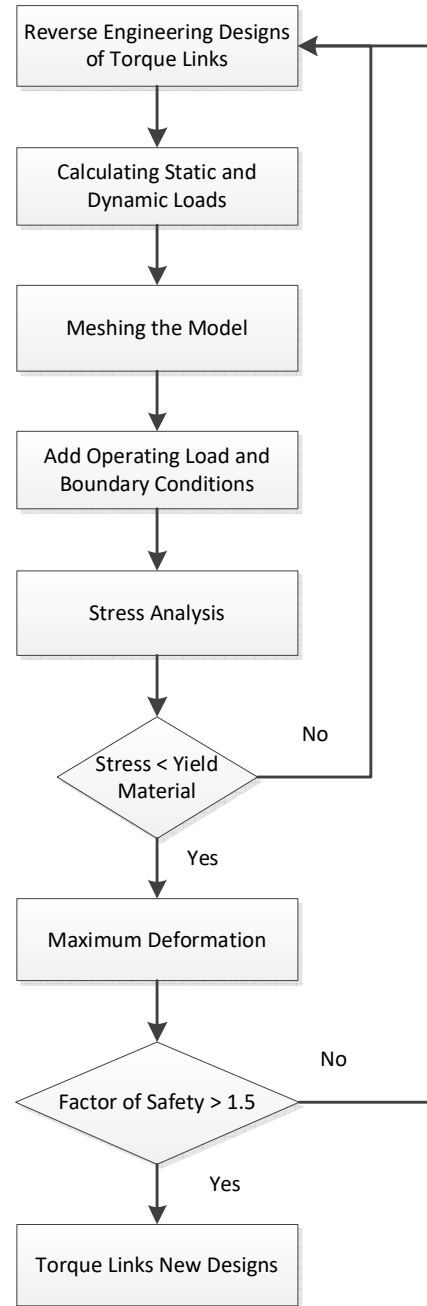


Fig. 4 Optimization design torque link

The torque links component can be modeled as simply supporting a beam of the shape and size shown in Figure 5. It is assumed that the area of the Torque Links subject to bending is a 95 mm long structure that ranges from 65 mm at the top and 48 mm at the bottom with the cross-section of the Torque Links having a rectangular shape.

$$b(x) = 48 + 2x \tan(5^\circ) \quad (6)$$

From the structure and loading, we see that the upper torsion relationship behaves as a simply supported beam with moments in the section connected to the nose cylinder. The diameter of the hole is 25 mm, and the distance between the centers of the holes is 30 mm.

Where thick $h = 25$ mm, the area of the section varies as:

$$A(x) = 25 \cdot [48 + 2x \tan(5^\circ)] \quad (7)$$

Moment of inertia of the section:

$$I(x) = \left(\frac{1}{12}\right) b h^3 \quad (8)$$

And because the width varies, so moment varies as:

$$I(x) = \left(\frac{1}{12}\right) b(x) 25^3 \quad (9)$$

Based on Hooke's Law, the theory of bending moments on a beam at any point x is given by the following equation:

$$-E I(x) \frac{d^2y}{dx^2} = M \quad (10)$$

$$-E I(x) \frac{dy}{dx} = Mx + C_1 \quad (11)$$

$$-E I(x) y(x) = \frac{Mx^2}{2} + C_1x + C_2 \quad (12)$$

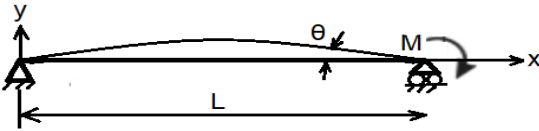


Fig. 5 Free Body Diagram of upper torque link

Referring to Figure 5 the deflection is zero ($y=0$) at the ends of the beam ($x=0$; $x=L$), so equation (12) can be obtained:

$$y(x) = -\frac{Mx^2}{2E I(x)} + \frac{MLx}{2E I(x)} \quad (13)$$

Equation (11) will be of maximum value if the derivative of the function is equal to zero ($y'=0$), at intervals of $0 \leq x \leq L$, so the maximum deflection is:

$$y\left(\frac{L}{2}\right)_{\max} = \frac{ML^2}{8E I\left(\frac{L}{2}\right)} \quad (14)$$

Stress at any point x can be calculated using Euler's equation:

$$\sigma(x) = \frac{M y(x)}{I(x)} \quad (15)$$

Where M is the moment, $y(x)$ is the deflection or distance from the neutral axis at the point x and $I(x)$ is the moment of inertia at that section.

Besides how much stress and deflection occur, it is important to determine the component's natural frequency to avoid any fatal accidents [8], [18]. This analysis can be done by studying the dynamic properties of the torque links under excitation through modal analysis. The work done by Kruger

and Morandini [19] gives a general outline of how vibration problems in landing gears can be treated by numerical methods.

The natural frequency of an object is that frequency with which any object will vibrate if disturbed and allowed to vibrate on its own without any external force:

$$\omega = \sqrt{\frac{k}{m}} \quad (16)$$

where k is stiffness and m is mass of the object respectively. An object can have an infinite natural frequency. To find the natural frequency and mode shapes we start with the equation of motion in matrix form. We have:

$$[M]\{X''\} + [C]\{X'\} + [K]\{X\} = \{F\} \quad (17)$$

where $[M]$, $[C]$, and $[K]$ are the mass, damping, and stiffness matrices. $\{X\}$ is the displacement vector and $\{F\}$ is the overall force acting on the system. For a free, undamped response we can set $[M]$, and $\{F\}$ to zero [9]. So, we have:

$$[M]\{X''\} + [K]\{X\} = 0 \quad (18)$$

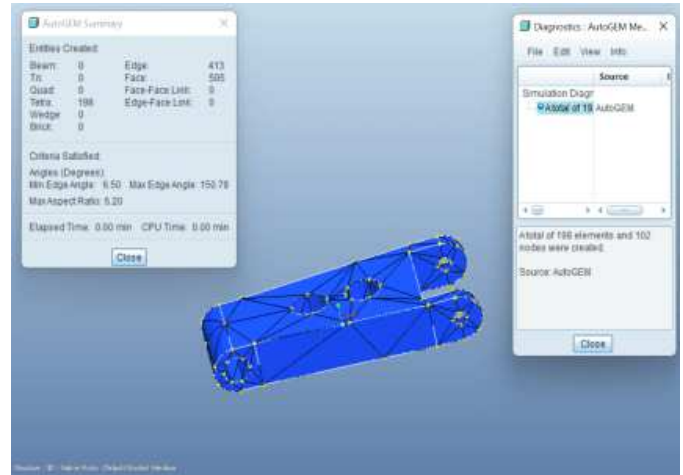


Fig. 6 Meshing process of upper torque link

The solid 3D CAD model of the torque link used for bending analysis and this model is meshed (tetra mesh) and the material properties were given using AutoGEM (Geometric Element Modeling) is shown in Figure 6. The properties material (6061-T6 Aluminum) used for torque links are shown in Table 1.

TABLE I
PROPERTIES OF ALUMINUM ALLOY (AL 6061)

| No | Properties | AL-6061 |
|----|---------------------------------|---------|
| 1 | Tensile Yield Strength [MPa] | 276 |
| 2 | Ultimate Tensile Strength [MPa] | 310 |
| 3 | Young's Modulus [MPa] | 68,900 |
| 4 | Shear modulus [MPa] | 26,000 |
| 5 | Density [kg/m3] | 2,700 |
| 6 | Poisson's ratio | 0.33 |

The best optimized CAD model of the torque link, obtained after the stress analysis, is used for modal analysis. This modal uses materials and properties that are the same as those used for stress analysis. Meshing is an important and critical step in finite element analysis and directly affects the complete process's outcome [20], [21].

Finite Element Method is one of the most powerful methods in numerical analysis techniques. The time-consuming tasks and high costs can be reduced by using this method in the early stages of machine component design [22]. The finite Element Method can be used to simulate and optimize material structure and simulate stress and deformation before making [23]. The first design in solid 3D of the torque links component of the nose landing gear is created using Pro/ENGINEER. After that, the FEM simulation process is made by the Mechanica Simulation application. Creating p-mesh for the Geometric Element Modeling mechanism was run using the AutoGEM tool. Before running the simulation analysis, create a Displacement Constraint with boundary condition and a Moment Load from the static and dynamic force. Utilizing an equivalent static load method, topology optimization with transient loads is performed to obtain optimal material distribution satisfying the objective function and constraints [5].

The results of a Finite Element Analysis are viewed using a Design Study, and the torque link's stress distribution is studied. Similarly, geometry is a change in AutoGEM for the second case, and the Mechanica Simulation process is repeated. The first set is done by moving the smaller hole away from the bigger hole by increasing center distances. However, the higher efficiency value obtained from the finite element analysis is based on the ideal condition as compared to the lower efficiency value obtained from the normal condition where several internal and external power losses might occur [24]. A modal analysis is done using Pro/ENGINEER, which is meshed using the AutoGEM tool, and its natural frequencies are found to analyze the different modes and shapes of vibration for different frequencies. An advanced iterative finite element method (FEM) is applied to estimate the amount of harvested energy [25].

III. RESULTS AND DISCUSSION

Static force (F_{static}) can be calculated from the Maximum Take-Off Weight (MTOW) of the aircraft (WL), which is distributed 15% on the nose landing gear in front (P_m) and 85% on the main landing gear in the rear [26]. This force occurs when the aircraft is at rest or not moving (F_{rest}). The static force will be countered by the shock absorber force (F_{shock}), and the difference will be transmitted to the torque link structure.

TABLE II
THE STATIC AND DYNAMIC MOMENT OF TORQUE LINK

| | | | | |
|-------------------|---------------------------|--------------------------|--------------------|------------|
| W_L [kg] | V_z [m/s ²] | g [kg/m ²] | N_g | h_t |
| 1,330 | 2.5 | 9.8 | 3 | 0.47 |
| S_t [mm] | h_s | P_m [kg] | F_{rest} [N] | k [N/mm] |
| 6.35 | 0.8 | 199.5 | 1,957.1 | 17.05 |
| S_s [mm] | S_{s_design} [mm] | F_{shock} [N] | F_{static} [N] | |
| 128.93 | 154 | 2,631.5 | -674.4 | |
| r [m] | M_{static} [Nm] | $E_{absorbed}$ [kg mm] | $F_{landing}$ [kg] | |
| 0.06 | -42.8 | 75,680.21 | 490.4 | |
| $F_{landing}$ [N] | $F_{dynamic}$ [N] | r [m] | $M_{dynamic}$ [Nm] | |
| 4810.6 | 2179 | 0.06 | 138.3 | |

Dynamic force can be calculated from the energy that can be absorbed by the shock absorber and the tires (Eabsorbed) when multiplied by the magnitude of the deflection of the shock absorber (S_{s_design}) will be the landing force ($F_{landing}$) [27]. The landing force will be countered by the shock absorber force (F_{shock}) with spring coefficient (k), and the difference is called dynamic force ($F_{dynamic}$) that will be transmitted to the torque link structure. The calculation of static-dynamic force if multiplied by the distance from force position to torque link (r) will be the static-dynamic moment that is tabulated in Table 2.

A. Bending Stress Results

The first set of results is obtained by changing the distance between the center of the holes, which increased from 30 to 60 mm. Stresses occur on the area near the hole that the center of moment loads, and maximum displacement is near almost the center of the torque link. The maximum stress that occurs is constant at 157.4 MPa. And the displacement trend is increasing, which is not very significant in small steps approaching 0.02 μ m. The bending stress does not change at a center distance of more than 30 mm. In this case, the mass of the torsion link remains the same.

The second set of results is done by increasing the hole diameter from 25 to 30 to 35 and finally, to 40 mm, and the center distance varied from 50 to 40 and finally to 45 mm. Increased hole diameter gives a reduction in stresses but causes displacement increase.

TABLE III
THE SIMULATION SET RESULTS

| Simulation Case | Hole diameter 1 [mm] | Hole diameter 2 [mm] | Hole diameter 3 [mm] | Center distance [mm] | Mass of torque link [kg] | Maximum Von Mises Stress [MPa] | Maximum Displacement [mm] |
|-----------------|----------------------|----------------------|----------------------|----------------------|--------------------------|--------------------------------|---------------------------|
| 1 | 20 | 20 | - | 30 | 0.393688 | 157.4 | 0.01615 |
| 2 | 20 | 20 | - | 40 | 0.393688 | 157.4 | 0.01616 |
| 3 | 20 | 20 | - | 50 | 0.393688 | 157.4 | 0.01616 |
| 4 | 20 | 20 | - | 60 | 0.393688 | 157.4 | 0.01617 |
| 5 | 25 | 25 | - | 50 | 0.369831 | 157.4 | 0.01634 |
| 6 | 30 | 30 | - | 40 | 0.340673 | 157.4 | 0.01656 |
| 7 | 35 | 35 | - | 45 | 0.306214 | 157.3 | 0.01742 |
| 8 | 40 | 40 | - | 45 | 0.266453 | 157.3 | 0.02018 |
| 9 | 20 | 25 | 30 | 60 | 0.334046 | 157.4 | 0.01660 |
| 10 | 20 | - | 30 | 60 | 0.300178 | 155.0 | 0.01671 |

The final simulation test is done by combining two holes of diameter 20 and 30 mm with a center distance of 60 mm. This can reduce mass, but the maximum stress that occurs is still within safe limits, and this is a better design than the previous one. The simulation results have been tabulated and shown in Table 3. And the results are plotted below in Figure 7.

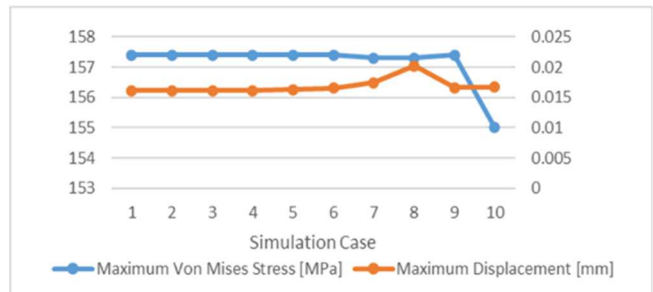


Fig. 7 Variation in stresses and displacement with 10 simulation cases

The final simulation test was done by putting 3 holes with 30-, 25-, and 20-mm hole diameter. The center distance between the smaller hole and the bigger hole is 60 mm. This helps in a further increase in the mass of torque link reduction. We see the maximum stress is 157.4 MPa and displacement

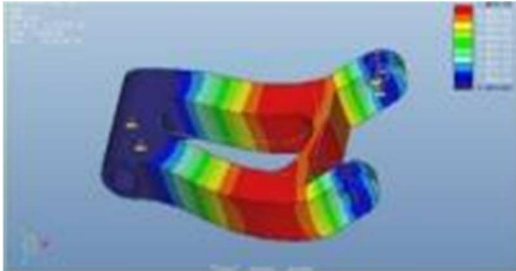
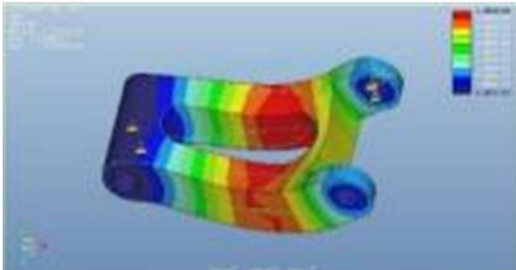
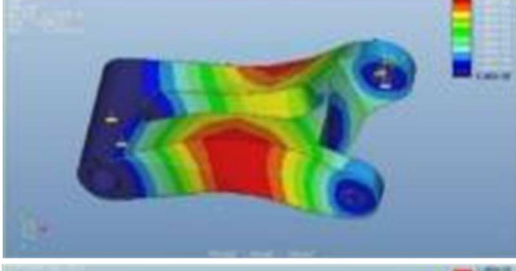
is 0.0166 mm. This can reduce the mass of the torque link more significantly, and the strength of the structure is still below the safe limit or yield strength, hence it is a desirable design.

B. Modal Analysis Results

The different mode shapes were obtained for four modes, their respective frequencies, and planes of deformation are shown below in Table 4. The natural frequencies obtained are

tabulated. The mode shapes show bending at the middle of the torque link in most cases. The value of the first mode is 4.2259 kHz below 5 kHz. It is seen to rise, and the rate of increase keeps rising till mode 4 with values 5.3992 kHz, 6.0459 kHz, and the last modal frequency is 6.1319 kHz. These values are important parameters in deciding the resonance characteristics of the component. The forcing frequencies must be free from these natural frequency values.

TABLE IV
THE MODAL ANALYSIS RESULTS

| Mode Shapes | Natural Frequency [kHz] | Plane of deformation | Simulation Results |
|-------------|-------------------------|----------------------|--|
| Mode 1 | 4.2259 | Bending in XY plane |  |
| Mode 2 | 5.3992 | Bending in XY plane |  |
| Mode 3 | 6.0459 | Bending in XZ plane |  |
| Mode 4 | 6.1319 | Bending in XZ plane |  |

IV. CONCLUSION

Based on the simulation results, the maximum von misses stress occurs near the hole area which is the connection part to the nose cylinder where the center of the moment is due to static and dynamic loads when the aircraft lands. This stress is dangerous for the structure and must be reduced because can affect the material strength of the landing gear and causes the bending stress on landing gear components in the torque link. From these simulation results obtained optimal design by combining the holes at the torque link, which will make

the weight lighter, but caused the strength to decrease. The best design, from simulation in case 10 can be achieved by combining two or more holes. This case has the least mass, only 0.300178 kg and a relatively very low value of the maximum stress is 155 MPa. And from this model continued for modal analysis, the natural frequency of vibration of different mode shapes obtained ranges from 4.2259 kHz to 6.1319 kHz, and this is still below the limit of 0.1 kHz (around 6,000 rpm engine). The research results obtained an optimal design with a safe structural strength, and the Factor of Safety is 1.78 (> 1.5).

NOMENCLATURE

| | | |
|-----------|---|------------------|
| Eabsorbed | The energy that can be absorbed by the shock | kg |
| WL | Weight of the aircraft at landing (MTOW) | kg |
| Ng | The landing gear load factor Ng = 3 (for Aircraft type: General aviation) | |
| ht | Tyre efficiency ht = 0.47 [4] | |
| St | The tire deflection St = 0.25 inch (for bias-ply, Static load 1800 Lbs [5]) | inch |
| hs | Shock absorber efficiency Hs = 0.8 (for Shock Absorber type: Oleo-pneumatic [4]) | |
| Ss | The shock absorber stroke | m |
| Vz | Design touchdown rates Vz = 8.2 fps (FAR 23: 7 – 10 fps) | fps |
| g | Acceleration due to gravity g = 9.81 m/s ² | m/s ² |
| ns | number of main gear struts | |
| Pm | The maximum static load per main gear | kg |

ACKNOWLEDGMENT

Some parts of the study in this article publication was conducted at the Agency for the Assessment and Application of Technology (since 2021 changed to the National Research and Innovation Agency) in Puspiptek Serpong, Indonesia between January 2021 and June 2022. The authors thank the Agencies and research members for the development of retractable landing gear for unmanned aircraft for supporting this study.

REFERENCES

- [1] N. Raičević, A. Grbović, G. Kastratović, N. Vidanović, and A. Sedmak, "Fatigue life prediction of topologically optimized torque link adjusted for additive manufacturing," *Int J Fatigue*, vol. 176, p. 107907, 2023, doi: <https://doi.org/10.1016/j.ijfatigue.2023.107907>.
- [2] P. Thota, B. Krauskopf, and M. Lowenberg, "Interaction of torsion and lateral bending in aircraft nose landing gear shimmy," *Nonlinear Dyn*, vol. 57, pp. 455–467, 2009.
- [3] C. Douglas, A. Ellis, R. K. Schmidt, and I. Kim, "Multidisciplinary Design Optimization of Aircraft Landing Gear," in *AIAA Aviation 2021 Forum*, 2021, p. 3023.
- [4] M. Rahmani and K. Behdinan, "Interaction of torque link freeplay and Coulomb friction nonlinearities in nose landing gear shimmy scenarios," *Int J Non Linear Mech*, vol. 119, p. 103338, 2020, doi: [10.1016/j.ijnonlinmec.2019.103338](https://doi.org/10.1016/j.ijnonlinmec.2019.103338).
- [5] M. Rahmani and K. Behdinan, "Structural design and optimization of a novel shimmy damper for nose landing gears," *Structural and Multidisciplinary Optimization*, vol. 62, no. 5, pp. 2783–2803, 2020, doi: [10.1007/s00158-020-02628-x](https://doi.org/10.1007/s00158-020-02628-x).
- [6] S. Singh, R. Chaudhary, V. K. Pathak, and V. Saxena, "Design Optimization of Torque Link of an Aircraft Landing Gear Assembly," in *Advances in Materials and Mechanical Engineering*, C. Pandey, V. Goyat, and S. Goel, Eds., Singapore: Springer Singapore, 2021, pp. 145–153.
- [7] Y. Jiang, G. Feng, P. Liu, L. Yuan, J. Ding, and B. Jiang, "Influence of Nose Landing Gear Torsional Damping on the Stability of Aircraft Taxiing Direction," *Aerospace*, vol. 9, no. 11, Nov. 2022, doi: [10.3390/aerospace9110729](https://doi.org/10.3390/aerospace9110729).
- [8] A. Krishnan, V. Thejus, and B. M. Arjun, "Numerical investigation of structural design of torsion links in a landing gear retraction mechanism," in *2017 2nd International Conference for Convergence in Technology (I2CT)*, IEEE, 2017, pp. 382–388.
- [9] M. Mahardika, R. A. Wicaksono, M. G. Widiastuti, and B. Arifvianto, "Finite Element Analysis of Osteosynthesis Miniplate for the Reconstruction of Parasymphseal Compound Fracture," vol. 8, no. 3, 2018.
- [10] M. Minhat, S. B. Mohamed, M. S. Kasim, M. A. Sulaiman, and Z. I. Rizman, "Advanced manufacturing of an aircraft component (fish-head): A technology review on the fabrication," *Int J Adv Sci Eng Inf Technol*, vol. 6, no. 5, pp. 734–739, 2016.
- [11] Y. Yin, K. Xu, H. Nie, X. Wei, and H. Wang, "Dynamics analysis of spatial landing-gear mechanism with hinge clearance and Axis deviation," *J Aircr*, vol. 58, no. 1, pp. 30–42, 2021.
- [12] L. Cheng, H. Cao, and L. Zhang, "Two-parameter bifurcation analysis of an aircraft nose landing gear model," *Nonlinear Dyn*, vol. 103, no. 1, pp. 367–381, 2021, doi: [10.1007/s11071-020-06129-w](https://doi.org/10.1007/s11071-020-06129-w).
- [13] L. Lin, C. Tong, F. Guo, S. Fu, Y. Lv, and W. He, "A Self-Attention Integrated Learning Model for Landing Gear Performance Prediction," *Sensors*, vol. 23, no. 13, p. 6219, 2023.
- [14] L. Son, K. E. Adipta, and M. Bur, "Analysis of the static behavior of a new landing gear model based on a four-bar linkage mechanism," *Int. J. Technol*, vol. 10, 2019.
- [15] Y. Jiang, G. Feng, P. Liu, L. Yuan, J. Ding, and B. Jiang, "Evaluation of Joint Clearance Effects on the Shimmy of Nose Landing Gear," *Aerospace*, vol. 10, no. 8, p. 722, 2023.
- [16] J. A. Griffin and T. T. Takahashi, "A Break from Tradition: The 'New' 14 CFR Part 23 and Consensus Standards," in *AIAA Scitech 2023 Forum*, 2023, p. 0116.
- [17] L. Miller and R. Jansen, "Structural Requirements for Design and Analysis of 25% Scale Subsonic Single Aft Engine (SUSAN) Research Aircraft," in *AIAA Scitech 2023 Forum*, 2023, p. 1939.
- [18] Z. Wu, "Modeling and simulation of aircraft nose landing gear extension retraction system," in *Proc.SPIE*, Sep. 2022, p. 122615A. doi: [10.1117/12.2638894](https://doi.org/10.1117/12.2638894).
- [19] W. R. Krüger and M. Morandini, "Recent developments at the numerical simulation of landing gear dynamics," *CEAS Aeronaut J*, vol. 1, pp. 55–68, 2011.
- [20] H. Borouchaki and P.-L. George, "Quality mesh generation," *Comptes Rendus de l'Académie des Sciences-Series IIB-Mechanics*, vol. 328, no. 6, pp. 505–518, 2000.
- [21] G. Balarac *et al.*, "Tetrahedral remeshing in the context of large-scale numerical simulation and high performance computing," *Mathematic.S In Action*, vol. 11, no. 1, pp. 129–164, 2022, doi: [10.5802/msia.22](https://doi.org/10.5802/msia.22).
- [22] M. A. Ahmad, N. N. M. E. Zulkifli, S. Shuib, S. H. Sulaiman, and A. H. Abdullah, "Finite Element Analysis of Proximal Cement Fixation in Total Hip Arthroplasty," *International Journal of Technology*, vol. 11, no. 5, pp. 1046–1055, Nov. 2020, doi: [10.14716/ijtech.v11i5.4318](https://doi.org/10.14716/ijtech.v11i5.4318).
- [23] S. Echaroj, N. Pannuchareonwong, and P. Rattanadecho, "Development of Vehicle Chassis from Novel Materials for Light Weight Electric Shuttles Using Finite Element Analysis," *Science & Technology Asia*, vol. 26, no. 3, doi: [10.14456/scitechasia.2021.47](https://doi.org/10.14456/scitechasia.2021.47).
- [24] M. N. Zulkifli, I. Ilias, A. Abas, and W. M. W. Muhamad, "Finite element analysis of thermoelectric generator with aluminum plate for waste heat recovery application," *Int J Adv Sci Eng Inf Technol*, vol. 7, no. 4, pp. 1328–1333, 2017.
- [25] M. Akbar *et al.*, "Evaluation on Piezoaeroelastic Energy Harvesting Potential of A Jet Transport Aircraft Wing with Multiphase Composite by means of Iterative Finite Element Method," *Evaluation*, vol. 13, no. 4, 2022.
- [26] F. Nikodem, F. Möller, P. Gallun, and A. Bierig, "Design of a retractable landing gear for the sagitta demonstrator UAV," 2017.
- [27] E. Satria, S. Haris, and R. Saputri, "Static and Dynamic Analysis of Steel U-Damper for Space Structures," vol. 8, no. 1, 2018.